Journal of Mines, Metals and Fuels, *71(12C) : 168-176; 2023. DOI: 10.18311/jmmf/2023/47298*

Print ISSN : 0022-2755

Journal of Mines, Metals and Fuels

Contents available at: *www.informaticsjournals.com/index.php/jmmf*

# A Non-Linear Study of Viscous Dissipation and Joule Effect on MHD Non-Newtonian Nanomaterial Flow over an Exponential Stretching Sheet with Heat Sink/ Source and Chemical Reaction

**P. A. Dinesh[1*], R. Sumithra[2], M. Jyothirmayi[3], Sweeti Yadav[1], K. R. Roopa[1], U. Shalini[2], V. Bhavya[2], C. Laxminarasamma[2] and S. M. Venkatalakshmi[2]**

*[1]Department of Mathematics, M S Ramaiah Institute of Technology, Bengaluru – 560054, Karnataka, India; dineshdpa@msrit.edu, sweetiyadav1989@gmail.com, krroopa870@gmail.com*

*[2]Department of Mathematics, Nrupathunga University, Bengaluru – 560054, Karnataka, India;sumitradiya@yahoo.com, shaliniu154@gmail.com, bhavyav127@gmail.com, lakshmigc337@gmail.com, venkatalakshmism044@gmail.com*

*[3]Department of Electronics and Instrumentation Engineering, M. S. Ramaiah Institute of Technology, Bangalore - 560054, Karnataka, India*

## Abstract

*This analysis presents the viscous flow of nanomaterials across a nonlinear stretching sheet in the boundary layer when there is a magnetic field. Rather than considering no slip conditions at the interface, velocity and thermal slip conditions are taken into account. The controlling partial differential equations are converted into non-linear ordinary differential equations by means of a similarity transformation set. The simplified equations are numerically solved using the shooting technique. The influence of controlling parameters on the mass diffusion of nanoparticles, temperature, speed, local mass transfer Sherwood number, Nusselt number, and drag coefficient is examined. It is discovered that while mass transfer increases, flow velocity, skin friction, and heat transfers decrease as the velocity slip parameter increases. The rates of mass and heat transmission decrease as the thermal slip parameters are increased. Graphical representations of the results are provided.*

**Keywords:** *Chemical Reaction, Joule Heating, MHD, Non-Newtonian Fluids, Viscous Dissipation*

## 1.0 Introduction

Magnetohydrodynamics (MHD) defines the motion of a conducting fluid with an applied magnetic field and is beneficial in boundary layer flows to regulate momentum and heat transfer across a stretched sheet. Major uses for an electrically conducting fluid include nuclear processes, polymer technologies, and metallurgy. The peculiar characteristics of nanomaterials are caused by the existence of zinc (Zn), Copper (Cu), manganese (Mn), iron (Fe), titanium dioxide (Ti) and other metallic nanoparticles. In 2013, Mukhopadhyay[1] examined numerical solutions for heat transfer and steady MHD boundary layer flow across an exponentially extended surface contained in a thermally stratified medium when suction is present. It was demonstrated that the impact of suction and

**Author for correspondence*

magnetic parameters on a viscous incompressible fluid is to suppress the velocity field, resulting in an increase in the skin-friction coefficient. An exponent extensible sheet was used to analyse the impact of velocity and thermo slip situations in an unstable 3 D MHD flow by Hayat *et al.*[2]. Zaimi *et al.*[3] investigated how radiation affected flow of a viscous fluid in an MHD boundary layer over a sheet that was stretching exponentially. It was discovered that when magnetic and radiation parameter values increase, the rate of local heat transfer at the surface decreases. The effect of solar radiation upon MHD thermal flux across permeable pathways was examined and numerically resolved using numerical approach by Yadav *et al.*[4].

Recent years have seen a rise in scientific interest in non-Newtonian fluids because of their many uses in industrial and technical settings. The applications of non-Newtonian fluids are numerous in a variety of chemical and biological processes, including the production of condensed milk, chocolates, ketchup, magma, sauces, and ice flows, as well as detergents, pharmaceutical chemicals, drilling mud, shampoos, and paints. The Casson fluid is a non-Newtonian fluid with yield stress. The fluid behaves like a solid if the applied shear stress is less than the yield stress. The fluid begins to flow if the applied shear stress exceeds the yield stress and the fluid starts to move. Jelly, tomato sauce, blood, concentrated juices, honey and other substances are typical examples of Casson fluid. The computational solution for border layer MHD mass and heat transport across a curved sheet having the presence of a Casson fluid was given by Roopa *et al.*[5].

One of the best rheological models for studying boundary layer flows is the Casson model. The implications of solar radiation on Casson fluid movement and transfer of heat via an exponentially porosity stretchable surface were discussed numerically by Pramanik[6]. 3D magneto-Casson fluid movement on a permeable stretchable sheet having convection boundaries was studied by Mahanta and Shaw[7]. Mahdy examined the thermal and mechanical properties of not a Newtonian Casson liquids flowing through an upward extending surface in an unstable MHD boundary layer with slip flow, taking into consideration the impacts of heat production or absorbance and suction/injection. Casson invented the Casson fluid in 1859. It makes the yielding stress visible. It behaves like a solid whenever shear stress is low yet acts like a liquid otherwise. Examples of Casson fluid include colour, tomato-based jam, honey, strong juice from fruits, and soup. Pramanik[6] provided an illustration of the heat transmission flow across a stretched sheet with electromagnetic radiation, noting that increasing Casson parameter values increase surface stress. Hayat *et al.*[2] and Nadeem *et al.*[8] examined the MHD heat transfer Casson fluid past a stretched sheet in the midst of a field of magnets. The convection movement of MHD towards an expanded sheet due to slip Consequences was covered by Raju *et al.*[9]. They came to the conclusion that increasing the value of the magnetic field parameter diminishes skin friction and the Nusselt number.

Ullah *et al.*[10] quantitative investigation looked at how a chemical reaction caused by irregular cylinder elongation affected the MHD slip movement in Casson liquid. Hussain et al. explored the MHD combination of convection and heat exchange of an unconventional Casson fluid through a permeable extended blade in 2021. Bhavana *et al.*[11] investigated the movement of an impermeable, unconventional fluid under its presence of MHD, a porous material that transfers heat. Other unconventional fluid that may be employed at both high and low viscous rates of shear is the Carreau solvent. The transfer of heat and flow through the boundary layer to a Carreau system on a not linear extending surface are investigated by Hashim *et al.*[12].

Irfan[13] investigated the consequences of several slips, Brownian movement, and thermophoresis on the MHD motion of a Carreau nanofluid across a radiated extended sheet. Machireddy and Naramgari[14] examined the heating energy and transfer of mass characteristics of the MHD Carreau flow 3D movement via a perforation stretchable sheet, accounting for the impact of cross dispersion and Hall current. Shah *et al.*[15] investigate the MHD effect on the Carreau flow of fluid across an irregular shrinking surface by means of convection heat transfer.

The goal of this work is to conduct a non-linear investigation of joule heating and viscous dissipation on MHD Casson-Carreau fluid flow across an exponential stretching sheet that includes a chemical reaction and heat sink/source.

## 2.0 Mathematical Formulation

Assume a continuous, incompressible, two-dimensional flow of Carreau and Casson streams in the direction of an exponential expanding surface. The y-axis, on the other hand, is perpendicular to the outer layer and the x-axis is

passed via an elastic sheet in the plane of flow. In the x-axis, the exponential sheet of expansion is assumed with velocity $U_W = Ue^{\frac{Nx}{L}}$ elucidate at $y = 0$, where exponential parameter is *N* and length is *L*. The current concept is thought to address the Casson flow and Carreau flow when $n = 1$ and when $\beta \to \infty$ respectively. Brownian motion phenomena and thermophoresis are also taken into account. As seen in Figure 1, $B_0$ is taken in y direction.

The governing boundary layer equations are as follows, based on the above-mentioned as Kumar MS *et al.*[16]:

$$\frac{\partial u}{\partial x} + \frac{\partial v}{\partial y} = 0 \tag{1}$$

$$U\frac{\partial u}{\partial x} + V\frac{\partial u}{\partial y} = \nu\left(1 - \frac{1}{\beta}\right)\frac{\partial^2 u}{\partial y^2} + \frac{3\nu(n-1)\Gamma^2}{2}\left(\frac{\partial u}{\partial y}\right)^2\frac{\partial^2 u}{\partial y^2} - \frac{\sigma B_x^2}{\rho_f}u \tag{2}$$

$$\frac{\partial T}{\partial x} + v\frac{\partial T}{\partial y} = \alpha\frac{\partial^2 T}{\partial y^2} + \tau\left[D_B\frac{\partial c}{\partial y}\frac{\partial T}{\partial y} + \frac{D_T}{T_\infty}\left(\frac{\partial T}{\partial y}\right)^2\right] + \frac{\mu}{\rho C_p}\left(\frac{\partial u}{\partial y}\right)^2 + \frac{Q_0}{\rho C_p}(T - T_\infty) - \frac{\sigma B_0^2 U^2}{\rho_0 C_p} \tag{3}$$

$$\frac{\partial c}{\partial x} + v\frac{\partial c}{\partial y} = D_B\frac{\partial^2 c}{\partial y^2} + \left(\frac{D_B}{T_\infty}\right) + \frac{\partial^2 T}{\partial y^2} + \gamma(c - c_\infty)^n \tag{4}$$

Here $u$, $v$ represents the velocity components in the *x*, *y* directions respectively, $\rho_f$ - fluid flow density, $\nu$ - kinematic viscosity, $k^* = k_0 e^{-\frac{Nx}{L}}$ represent the permeability, $k_0$ is constant which gives initial permeability, $\sigma$ -electric conductivity, $\tau$ - material constant, $(\rho C)_f$ - heat capacity, $c$ - fluids concentration, $(\rho C)_p$ - heat capacity with fixed pressure, $\tau = \frac{(\rho C)_p}{(\rho C)_f}$, $\alpha = \frac{\kappa}{\rho C_f}$ - thermal diffusivity, $T$ - Temperature, $T_\infty$ - ambient temperature , $D_\infty$ - Brownian diffusion, $\beta$ - Casson parameter, and $D_T$ - thermophoresis diffusion. $B(x) = B_0 e^{\frac{Nx}{2L}}$, applied magnetic field where $B_0$ being constant.

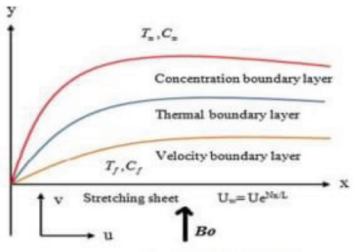



**Figure 1.** Physical model.

Subjected boundary conditions are:

$$\left.\begin{aligned} D_B\frac{\partial c}{\partial y} + \frac{D_T}{T_\infty}\frac{\partial T}{\partial y} = 0 \text{ at } y = 0 \\ -\kappa\frac{\partial T}{\partial y} = h_f(T_f - T), u = U, v = 0, \\ u \to 0, v \to 0, \\ T = T_\infty, c = c_\infty \text{ as } y \to \infty \end{aligned}\right\} \tag{5}$$

The classification of the similarity transformations is:

$$\left.\begin{aligned} u = U_W = Ue^{\frac{Nx}{L}}f'(\eta),\ \eta = y\sqrt{\frac{U}{2\nu L}}e^{\frac{Nx}{L}}, \\ \mathrm{v} = -\sqrt{\frac{\nu U}{2L}}e^{\frac{Nx}{2L}}\{f(\eta) + \eta f'(\eta)\} \end{aligned}\right\} \tag{6}$$

Equation (1), which is automatically fulfilled, using (6), (2-4) then converted to

$$\left(1 + \frac{1}{\beta}\right)f''' + N\left[ff'' - 2(f')^2\right] + \frac{3(n-1)}{2}We\,f'''(f'')^2 - Mf' = 0 \tag{7}$$

$$\theta'' + \frac{N\,\mathrm{Pr}}{1+R}(f'\theta' - \theta' f) + \frac{Nb}{1+R}\theta'\phi' + \frac{Nt(\theta')^2}{1+R} + \frac{\mathrm{Pr}\,Ec}{1+R}\frac{(f'')^2}{(f')^2} - \frac{M\,\mathrm{Pr}\,Ec}{1+R} + \frac{\mathrm{Pr}\,\alpha\,\theta 2\nu Lf'}{U_W(1+R)} = 0 \tag{8}$$

$$\theta'' + Sc\,N[f'\theta' - \theta' f] + \frac{Nt}{Nb}\phi'' + \frac{Sc\,\gamma(c - c_\infty)^{n-1}f'(\phi)^n}{U_W} = 0 \tag{9}$$

with boundary conditions

$$f(0)=0, f'(0), \theta'(0)=-Bi(1-\theta(0)), \quad Nb\phi'(0)+Nt\,\theta'(0)=0 \tag{10}$$

$$f'(\eta)\to 0, \theta(\eta)\to 0, \phi(\eta)\to 0 \; as \; \eta\to\infty \tag{11}$$

Where $M=\frac{2\sigma B_0^2 L}{U_\rho}$ is magnetic parameter, $W_e=\frac{U^3 e^{3N_x/L}}{\vartheta L}$ Ã² is Weissenberg number, $Pr=\frac{\vartheta}{\alpha}$ is Prandtl number, $Nt=\frac{D_T(T_f-T_\infty)(\rho C)_p}{T_\infty\,\vartheta(\rho C)_f}$ is the thermophoresis parameter, $Nb=\frac{D_B C_\infty(\rho C)_p}{\vartheta(\rho C)_f}$ is the Brownian motion is parameter, $Sc=\frac{\vartheta}{D_B}$ is Schmidt number, $Ec=(U_w^2)/((T_w-T_?)C_{(p)})$ $Ec=\frac{U_w^2}{(T_w-T_\infty)C_p}$ is Eckert number.

Nusselt number and drag coefficient are as follows

$$\sqrt{\frac{2}{R_e}}Nu_x=-\theta'(0), \tag{12}$$

$$\sqrt{R_e}Cf=\left(1+\frac{1}{\beta}\right)f''(0)+\frac{(n-1)W_e^2}{2}\left(f'(0)\right)^3, \tag{13}$$

where, local Reynolds number, $\mathrm{Re}=\frac{U_W L}{\nu}$.

## 3.0 Solution Procedure

The shooting technique is a numerical method used to solve Ordinary Differential Equations (ODEs) or boundary value problems by transforming them into initial value problems. It involves "shooting" an initial guess for the unknown variables and adjusting it iteratively until the desired boundary conditions are satisfied. Here's a basic overview of how the shooting technique works. If you have a boundary value problem, transform it into an initial value problem by guessing one boundary condition and treating the other as an unknown parameter. Make an initial guess for the unknown parameter(s) and solve the resulting initial value problem using a numerical ODE solver (e.g., Runge-Kutta methods) to obtain a solution. Compare the solution obtained from the initial value problem with the desired boundary condition that you didn't use for the initial guess. Once the answer has been achieved fits the required boundary condition within a given tolerance, adjust the estimated parameter and continue steps repeatedly. You have discovered a numerical solution to the initial boundary value problem after the solution converges to the required boundary condition. The success of the shooting technique depends on the initial guess and the behavior of the solution. It's a trial-and-error process that requires careful adjustments and convergence monitoring.

## 4.0 Results and Discussion

The graph compares two types of non-Newtonian fluids: Casson fluid and Carreau fluid. Casson fluid is a model for shear-thinning fluids that have yield stress, which means they behave like a solid until a certain amount of force is applied. Carreau fluid is a model for fluids that have different viscosities at high and low shear rates, but no yield stress. We demonstrated how the magnetic field variable, the exponential variable, the Biot number, the thermophoresis variable, the Brownian momentum, and the value of the Weissenberg number affected the mass diffusion, velocity, and heating fields. In addition, we calculated the surface friction and Nusselt number.

The graph in Figure 2 inset displays the variation of $\theta(\eta)$ for different amounts of *M*. For the Casson and Carreau fluids, $\theta(\eta)$ gradually drops to zero as $\eta$ increases. The variation of $\phi(\eta)$ with respect to various values of the Magnetic parameter is illustrated in Figure 3. For both the Casson and Carreau fluids, as $\eta$ rises steadily, $\phi(\eta)$ reaches its peak, and finally saturates. It is also evident from the inset graph that there are three sites at which the Casson and Carreau fluids connect. As the value of *M* increases, the concentration increases and the rate of mass transfer decreases.

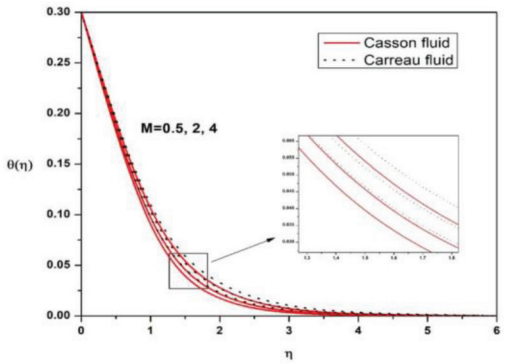



**Figure 2.** Consequences of *M* on temperature.

The velocity graph's fluctuation with regard to the magnetic parameter *M* is shown in Figure 4. The velocity boundary layer thickness grows with increasing values of the magnetic parameter M. The velocity graph's fluctuation with regard to the magnetic parameter is shown in Figure 4. The velocity boundary layer thickness grows with increasing values of the magnetic parameter M. This occurs because the transverse magnetic field introduces Lorentz force, which causes the velocity field to experience retardation. As a result, the retarding force rises in proportion to the quantities of M, which lowers the rate of speed.

Figure 5 shows the effect of Schmidt number on the concentration profile. It is seen that for both fluids concentration is reduced when $\eta < 1.5$, an *Sc* increase results in a reduction of the concentration's thickness. is really inversely proportional to mass diffusivity and directly proportional to momentum diffusivity; as a result, higher values of Sc are consistent with low mass diffusivity, which lowers the concentration function. It is noteworthy that a decrease in the concentration of nanoparticles is indicated by a change in Sc for $\eta > 1.5$. A decrease in solutal transmission, indicated by a change in Schmidt number, indicates a decrease in nanofluid concentration. Moreover, an increase in $\phi(\eta)$ from negative to positive is observed as $\eta$ increases. Figure 6 illustrates how the thermophoresis parameter affects the concentration field. The concentration boundary layer thickens increases as thermophoresis rises. Concentration distributions grow increasingly irregular. Similarly, non-uniformity in the concentration distribution is encouraged by thermophoresis, and this effect becomes more pronounced at much higher concentrations. The graph indicates that when η increases from a negative to a positive number, the value of changes. The fluctuation of Nt on the impacts of concentration profiles is revealed by the growing casson and carreau fluids. It is noticed that rising casson and

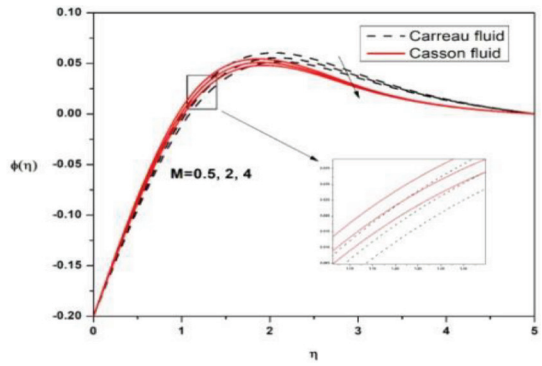



**Figure 3.** Consequences of *M* on concentration.

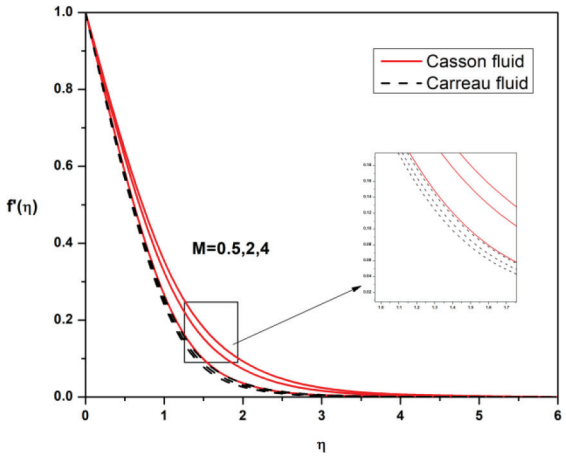



**Figure 4.** Consequences of *M* upon velocity.

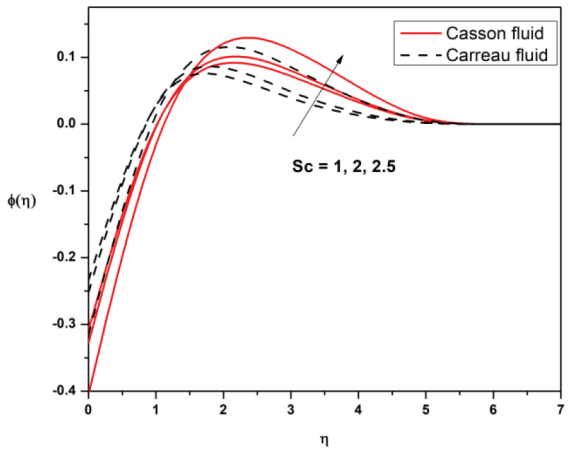



**Figure 5.** Consequences of *Sc* upon concentration.

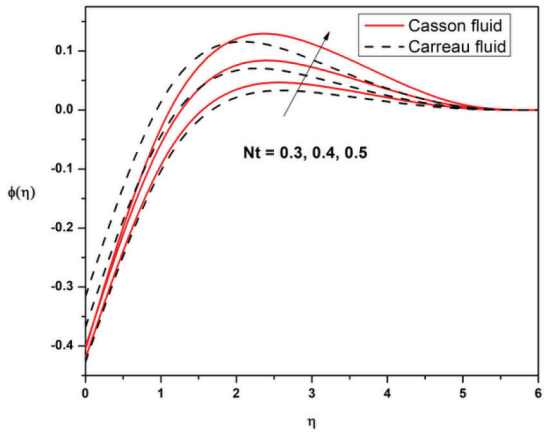



**Figure 6.** Consequences of *Nt* upon concentration.

carreau fluids values the curves are increasing as but they have different heights depending on the value of Nt.

Figures 7-9 present the consequences of *We* on rate of speed, mass diffusion and temperature fields. It is noted that fluid velocity and concentration (for both Casson and Carreau fluids) are decreasing functions of *We*, whereas the fluid temperature is an increasing function.

The Weissenberg number causes a decrease in the specified process time. Both the boundary layer thickness and fluid velocity decrease with a reduction in the specified process time. In terms of physics, the Weissenberg number has an inverse relationship with velocity and a direct relationship with the time constant. When the Weissenberg number values rise, the time constant to viscosity ratio increases. Weissenberg number hence increases velocity profiles while decreasing temperature and concentration fields.

Figures 10 and 11 are sketches to consequences of *J* on the temperature and concentration fields respectively. The temperature profile is increased with an increase in *J*. The fluid's temperature rises as a result of an increase in *J* the electrical conductivity and magnetic field intensity, which both boost current generation. The graph shows that both Casson and Carreau fluids have higher shear stress than Newtonian fluids at low shear rates, but lower shear stress than Newtonian fluids at high shear rates, the red curve represents the Casson fluid model, and the black curve represents the Carreau fluid model, the arrows on the graph indicate different values of J, which is a dimensionless parameter that represents the ratio of viscous force to elastic f in the force in the fluid. J = 0.5,2,4 are typical values for blood flow in arteries. The Casson and Carreau fluids are in the point of temperature the both fluids are very compressible to each other. The graph shows the relationship between a dimensionless parameter η and a function φ(η) for both

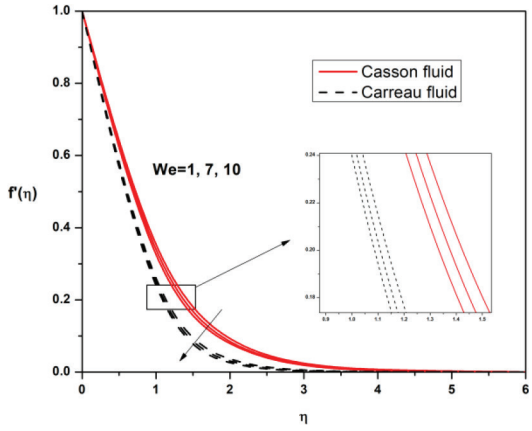



**Figure 7.** Consequences of *We* upon velocity.

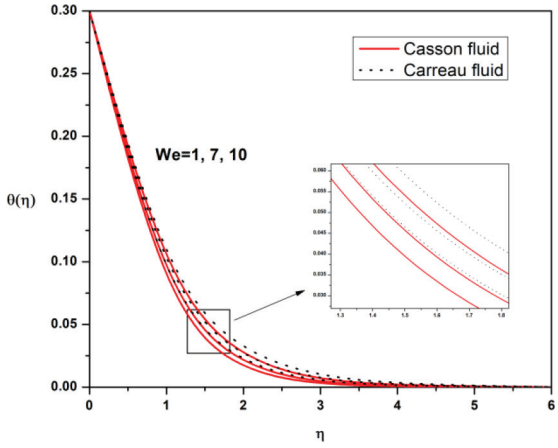



**Figure 9.** Consequences of *We* upon temperature.

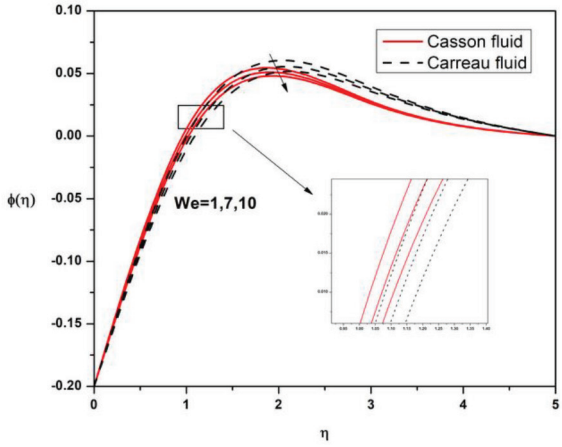



**Figure 8.** Consequences of *We* upon concentration.

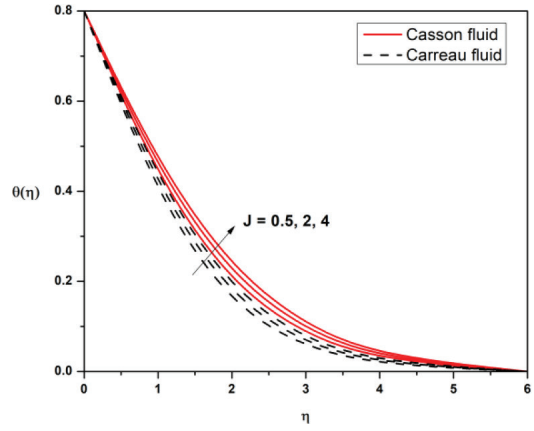



**Figure 10.** Consequences of *J* upon temperature.

Casson fluid and Carreau fluid. The function φ(η) is related to the velocity profile of the fluid in a pipe. The graph has two vertical lines at J = 0.5 and J = 2.4, which correspond to two different values of another dimensionless parameter J. This parameter J is related to the ratio of the pressure gradient to the yield stress for Casson fluid, and to the ratio of the pressure gradient to the zero-shear viscosity for Carreau fluid. The graph shows that for both Casson fluid and Carreau fluid, φ(η) increases as η increases, but at different rates. The red curve (Casson fluid) is smoother than the black curve (Carreau fluid), which has some jagged parts. The curves intersect at two points, one near the origin and one near the top right corner of the graph. The intersection points indicate that there are some values of η for which both fluids have the same value of φ(η).

Figures 12 and 13 show the influence of viscous dispersion, or Eckert number, across dimensionless temperature as well as concentration. They are found to be increased as a result of the dissipation repercussions. Furthermore, the thickness of the thermal boundary layer widens in the instance of the Carreau fluid, illustrating that the dissipative energies becomes more significant as the temperature goes up.

The graph (Figure 12) shows that for both fluids, $\phi(\eta)$ decreases as $\eta$ increases, which means that both fluids have a shear-thinning behavior. The graph (Figure 13) shows that Casson fluid has a higher peak value φ(η) than Carreau fluid.

The effects of the biot number upon mass diffusion and temperature curves are seen in Figures 14 and 15, respectively. An increasing Biot number suggests a rise in the heat transmission coefficient. The boost in the energy transfer causes the temperature to go up. It is clear that when Biot values for numbers climb, mass diffusion and temperature also rise.

It is also observed that increase in $\eta$ increases $\phi(\eta)$ and decreases $\theta(\eta)$ and there are intersection points in both the graphs which indicate that at certain points the concentration profile and velocity profile are same for both Casson and Carreau fluids.

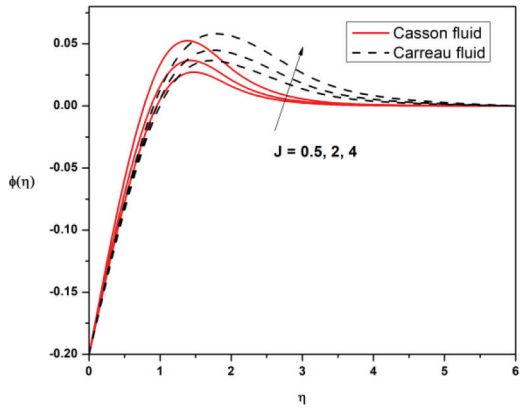



**Figure 11.** Consequences of *J* upon concentration.

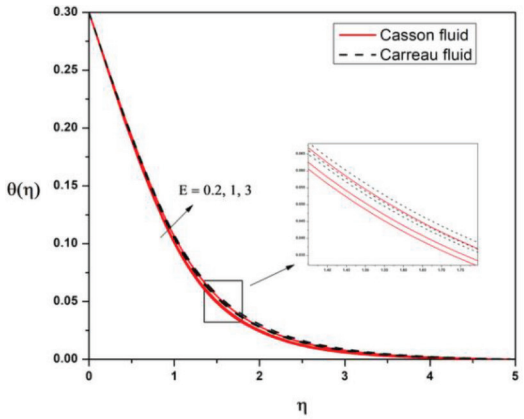



**Figure 12.** Consequences of *Ec* upon temperature.

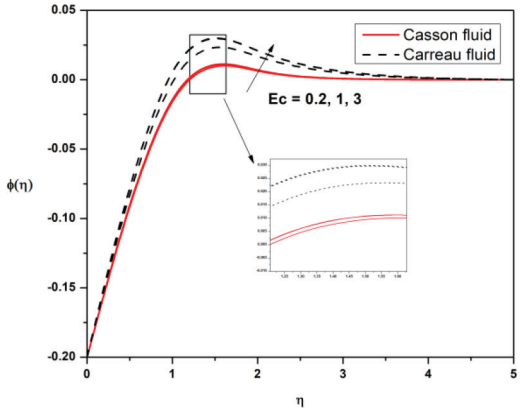



**Figure 13.** Consequences of *Ec* upon concentration.

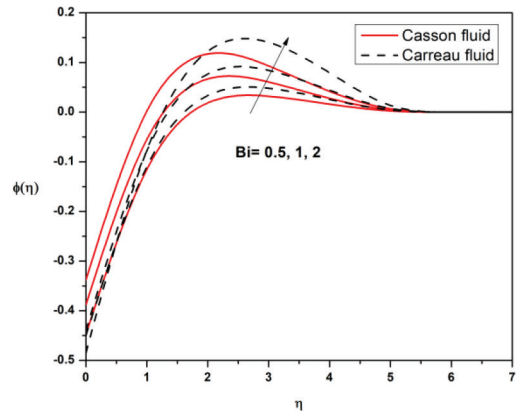



**Figure 14.** Consequences of *Bi* upon concentration.

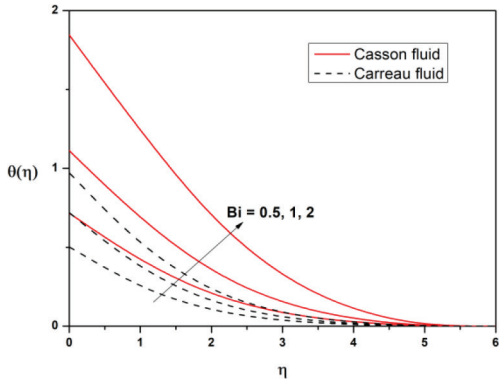



**Figure 15.** Consequences of *Bi* upon temperature.

## 5.0 Conclusion

In this work, we examine the heat and mass transfer associated with 2D MHD boundary layer Casson fluid flow across a stretching surface and its flow of the viscous incompressible non-Newtonian fluid having magnetic fields with the heat source/sink media is an analyzed under the viscous dissipation and Joule Consequences by using similar transformation. After being transformed into ODEs, the concentration and heat equation sets are solved using the fourth-order Runge-Kutta and firing techniques. The primary findings of this investigation are as follows:

For both parameter (M) and Schmidt number (Sc), the mass transfer gradient exhibits increasing behavior.

- When the Carreau fluid is paralleled with the Casson fluid, the Lorentz force has a significant impact on it.
- Positive values of heat source/sink parameter function as a heat generator.
- The parameters of thermophoresis and Brownian moment function similarly to those regulating concentration and temperature boundary layers.
- The exponential factor successfully increases the rate of transfer of heat of both fluids.
- The study sheds light on the migration of nanomaterials like metals, metal oxides, carbide particles, or carbon-based nanotubes.

## 6.0 References


1. Mukhopadhyay S. MHD boundary layer flow and heat transfer over an exponentially stretching sheet embedded in a thermally stratified medium. Alexandria Eng J. 2013; 52(3):259-65. https://doi.org/10.1016/j.aej.2013.02.003
2. Hayat T, Shehzad SA, Alsaedi A. Soret and Dufour effects on Magnetohydrodynamic (MHD) flow of Casson fluid. Appl Math Mech. 2012; 33(10):1301-12. https://doi.org/10.1007/s10483-012-1623-6
3. Zaimi K, Ishak A, Pop I. Boundary layer flow and heat transfer over a nonlinearly permeable stretching/shrinking sheet in a nanofluid. Sci Rep. 2014; 4(1):4404. https://doi.org/10.1038/srep04404
4. Yadav S, Dinesh PA, Roopa KR, Gogate SSP. Three-dimensional analysis of electromagnetic nanomaterial flow and thermal variations for forced convection. J Mines, Met Fuels. 2023; 71(10):1442-54. https://doi.org/10.18311/jmmf/2023/35810
5. Roopa KR, Dinesh PA, Yadav S, Govindaraju MV. Numerical technique for a Darcy-Forchheimer Casson CuO-MgO/methanol hybrid nanofluid flow due to an elongated curved surface with chemical reaction. J Mines, Met Fuels. 2023; 71(10):1431-41. https://doi.org/10.18311/jmmf/2023/35809
6. Pramanik S. Casson fluid flow and heat transfer past an exponentially porous stretching surface in presence of thermal radiation. Ain Shams Eng J. 2014; 5(1):205-12. https://doi.org/10.1016/j.asej.2013.05.003
7. Mahanta G, Shaw S. 3D Casson fluid flow past a porous linearly stretching sheet with convective boundary condition. Alexandria Eng J. 2015; 54(3):653-9. https://doi.org/10.1016/j.aej.2015.04.014
8. Nadeem S, Ul Haq R, Lee C. MHD flow of a Casson fluid over an exponentially shrinking sheet. Sci Iran. 2012; 19(6):1550-3. https://doi.org/10.1016/j.scient.2012.10.021
9. Raju CSK, Sandeep N, Sulochana C, Babu MJ. Dual solutions of MHD boundary layer flow past an exponentially stretching sheet with non-uniform heat source/sink. J Appl Fluid Mech. 2016; 9(2):555-63. https://doi.org/10.18869/acadpub.jafm.68.225.24784
10. Ullah M, Alkanhal TA, Shafie S, Nisar KS, Khan I, Makinde OD. MHD slip flow of Casson fluid along a nonlinear permeable stretching cylinder saturated in a porous medium with chemical reaction, viscous dissipation, and heat generation/absorption. Symmetry (Basel). 2019; 11(4):531. https://doi.org/10.3390/sym11040531
11. Bhavana PM, Vanitha GP, Mahabaleshwar US, Souayeh B. Effect of magnetohydrodynamic Casson fluid flow on the stretching/shrinking surface. ZAMM - J Appl Math Mech/Zeitschrift für Angew Math und Mech. 2023; 103(10). https://doi.org/10.1002/zamm.202200523
12. Hashim, Khan M, Ul Huda N, Hamid A. Non-linear radiative heat transfer analysis during the flow of Carreau nanofluid due to wedge-geometry: A revised model. Int J Heat Mass Transf. 2019; 131:1022-31. https://doi.org/10.1016/j.ijheatmasstransfer.2018.10.140
13. Irfan M. Study of Brownian motion and thermophoretic diffusion on non-linear mixed convection flow of Carreau nanofluid subject to variable properties. Surf Interfac. 2021; 23:100926. https://doi.org/10.1016/j.surfin.2021.100926

14. Machireddy GR, Naramgari S. Heat and mass transfer in radiative MHD Carreau fluid with cross diffusion. Ain Shams Eng J. 2018; 9(4):1189-204. https://doi.org/10.1016/j.asej.2016.06.012
15. Shah SAGA, Hassan A, Alsubaie N, Alhushaybari A, Alharbi FM, Galal AM, *et al*. Convective heat transfer in magneto-hydrodynamic carreau fluid with temperature dependent viscosity and thermal conductivity. Nanomaterials. 2022; 12(22):4084. https://doi.org/10.3390/nano12224084
16. Kumar MS, Sandeep N, Kumar BR, Dinesh PA. A comparative analysis of magnetohydrodynamic non-Newtonian fluids flow over an exponential stretched sheet. Alexandria Eng J. 2018; 57(3):2093-100. https://doi.org/10.1016/j.aej.2017.06.002